

Drag Reduction Using Spiked-Aerodisk & Reattachment Ring for Hypersonic Hemispherical Bodies

M. Elsamanoudy^{*}, A. Ghorab[†], and M. Hendy[‡]

Abstract: Rockets and Shuttles flying at hypersonic speeds experience severe drag and aerodynamic heating. While blunting the fore-body helps distribute the heat load over a large area, this produces, however, substantial amount of drag. A number of studies were dedicated to understanding the mechanism of drag and heat mitigation with spikes and maximizing the performance. This study aims at alleviating the severe pressure and heating occurring at the reattachment point by the introduction of the Reattachment Ring; a ring mounted at the reattachment point. Using the commercial code FLUENT, to solve the complicated flow field, this study seeks to maximize the amount of the total drag and heat reduction using spike-disk-spike assembly. The models are tested at Mach 6, 8 & 10 at altitude 25 km in standard atmosphere. The Reattachment Ring and the spike-disk-spike assembly add up synergistically to achieve a maximum drag reduction of 69.82%.

Keywords: drag reduction, hypersonic flow, CFD, spike, aerodisk, aerodynamic heating

Nomenclature

C_D	= drag coefficient
D	= diameter of blunt hemisphere, m
d	= diameter of the aerodisk, m
H	= height of the aerodisk, m
h	= height of the reattachment ring, m
k	= thermal conductivity, W/m.K
L	= spike length, m
P	= pressure, Pa
Re	= Reynolds number based on the diameter of the hemisphere
T	= temperature, K
t	= ring thickness, m
α	= semi-apex angle, °
θ	= the angle measured from the root of the spike in a clockwise direction, °
μ	= dynamic viscosity, N.s/m ²

Subscripts

w	= wall value
∞	= free stream value

* Professor of Fluid Mechanics and Turbomachines, Department of Mechanical Power Engineering, Ain Shams University, Cairo 11517, Egypt.

† Associate Professor of Fluid Mechanics and Turbomachines, Department of Mechanical Power Engineering, Ain Shams University, Cairo 11517, Egypt.

‡ M.Sc. Research Student, Department of Mechanical Power Engineering, Ain Shams University, Cairo, Egypt; Muhannad.Hendy@gmail.com .

1. Introduction

Spikes have been gaining popularity over the past decades as means of drag reduction for hypersonic blunt equipment. Although pointed cones have better aerodynamic characteristics than that of blunt noses, blunt noses are preferred over pointed cones at hypersonic speeds. Blunt noses have higher volumetric efficiency to accommodate the crew of manned equipment as well as radar and navigation devices. And because of their larger surface area, blunt noses can withstand more the extreme heating resulting at hypersonic flights without the need for overly-complicated thermal protection systems. It's from the paradigm of gaining the favored aerodynamic characteristics of a pointed cone nose and avoiding the high drag penalty of a blunt nose that spikes (sometimes called aerospikes) emerged.

Crawford [1], conducted a landmark experimental investigation on pointed sharp spikes of different lengths at Mach 6.8 and observed drag reduction for all spike lengths. He also pointed out that for Reynolds number less than 0.3×10^6 the flow behaves as laminar, and provided insights on the mechanism of drag reduction. Then instead of the sharp spike, an aerodisk mounted at the tip of the spike was proposed. Kukarni et al. [2] used a hypersonic wind tunnel to test the effectiveness of a flat aerodisk for drag reduction on a blunt cone of 120° apex angle. A consistent drag reduction of 57% was observed for the three flow stagnation enthalpies examined at Mach 8; this result affirmed that the drag reduction is independent of free stream Mach number and stagnation enthalpy. Khlebnikov [3] conducted an experimental study demonstrating the effect of rotating a spike (with an end cap) on the flow field around the hemispherical nose. He showed that by rotating the spike mechanical and thermal loads on the nose could be reduced.

In 2003, Hiroaki Kobayash et al. [4] proposed what they called Multi Row Disk (MRD). Zero-lift drag for the MRD device was found equal to the reference conical body and that it has better characteristics at non-zero angles of attack. The concept of pivoting spike was introduced by Erich Schülein [5] in which a self-aligning spike, using the weathercock principle, was tested at Reynolds number = 1.5×10^6 and for the angles of attack from zero to 30° . This configuration showed superiority over the fixed spike over the whole range of angles of attack achieving a drag reduction of 30% at 30° angle of attack. This configuration resulted, also, in a smoother heat flux distribution and lower heating.

Numerical investigations emphasizing the workings of spikes abound in the literature. MYM Ahmed & N. Qin [6,7] experimented on a variety of aerodisks shapes, using the commercial code FLUENT. The authors explained a mechanism of drag reduction based on the effective body shape. Flow instability around spiked bodies was addressed and the assumption of flow axi-symmetry was revisited. It was shown that the flow is asymmetric around the axis, however the bulk effects in terms of, for example, drag coefficient are the same assuming axi-symmetry. Gauer and Paull [8] tested numerically the effectiveness of aerodisks (which they called aerodomes). They achieved a maximum drag reduction of 63%.

It was observed that the use of spikes tend to cause very high heating at the blunt nose [1,6,7] which can pose a limitation to the wide application of spikes. Thus, in this work the authors aim at alleviating this problem by the introduction of the reattachment ring. It's, also, the aim of this study to try and achieve more drag reduction by the introduction of new spike assembly.

A fully numerical approach is adopted in this study to solve the Navier-Stokes equations around the selected models at high Reynolds numbers (4×10^6 : 6.67×10^6). The study starts by testing two conventional models at Mach 6 to demonstrate their limitations. Then, two new proposed configurations are tested and analyzed showing how they address successfully the above mentioned limitations.

2. Problem Setup

2.1. Geometry

2.1.1. Blunt Hemisphere

A blunt hemisphere of diameter 1 m is tested as a reference body.

2.1.2. Sharp Spike

A blunt hemisphere equipped with a sharp spike $L/D = 2$ and spike diameter $0.1D$. The semi-apex angle $\alpha = 10^\circ$, Fig. 1.

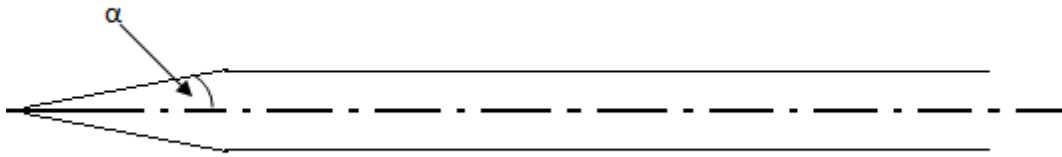


Fig. 1 Semi-apex angle, sharp spike.

2.1.3. Aerodisk-Equipped Spike

A blunt hemisphere equipped with a spike of diameter $0.05D$ at the end of it mounted a hemispherical aerodisk with $d/D = 0.1$. The spike/aerodisk assembly has a length ratio $L/D = 2.5$.

2.1.4. Spiked Aerodisk Assembly

A blunt hemisphere equipped with a conventional spike of diameter $0.1D$ and $L/D = 1$. Right at its end is mounted a cylindrical aerodisk with height $H = 0.125$ m and diameter $d = 0.138$ m. Another spike protrudes from this disk with Diameter = $0.1H$. The length of the whole spike-disk-spike assembly is $1.5D$. The reader may refer to Fig. 2 for a 3D view of this spike assembly.

2.1.5. Reattachment Ring

The authors proposed the concept of the reattachment ring, which is a ring mounted to the hemispherical nose with height $h = 0.1D$, and with thickness $t = 0.025$ –chosen arbitrarily. As the name suggests, this ring is mounted at the reattachment point where maximum pressure and heating occur. Figure 2 depicts the ring attached to the spiked aerodisk assembly.

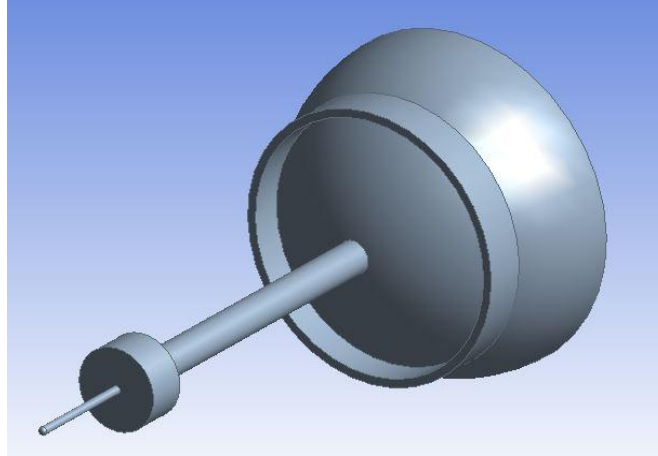


Fig. 2 3D view of the reattachment ring mounted to a hemisphere with spiked aerodisk.

2.2. Computational Mesh

An unstructured mesh is used. The domain is split in two regions: a region where high gradients exist and hence high resolution is required, and a region where the undisturbed flow remains unchanged. The near wall grid cells were adapted to conform to y^+ criterion in the range from 30 to 60 according to the recommendations given by Salim M. Salim and S.C. Cheah [9] for the Spalart-Allmaras turbulence model. Equation (1) defines the non-dimensional wall distance y^+ , where Δy_p is the distance to the near-wall node to the solid surface, ν is the kinematic viscosity, τ_w is the wall shear stress, and ρ is density of the fluid [10]. The cell count ranged from about 70,000 to 115,000 depending on the geometry and Reynolds number. The far field is imposed at $1/3D$ and $1D$ in the axial and radial directions [6], respectively.

$$y^+ = \frac{\Delta y_p}{\nu} \sqrt{\frac{\tau_w}{\rho}} \quad (1)$$

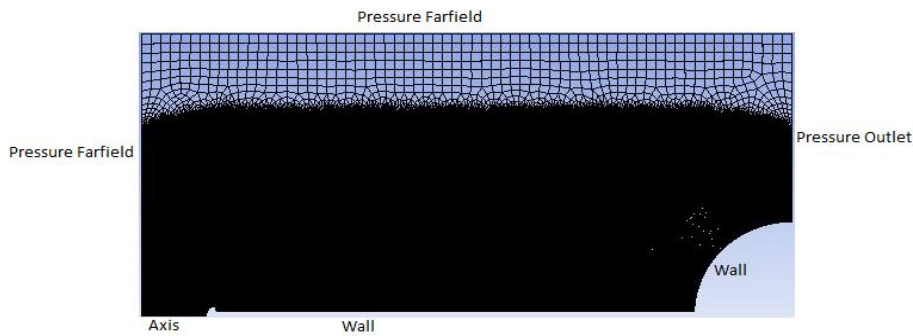


Fig. 3 Grid used with boundaries labeled.

2.3. Boundary Conditions

The type of boundary conditions is shown in Fig. 3. The different models are tested at an altitude of 25 km in US Standard Atmosphere [11]. At such an altitude, the free stream temperature $T_\infty = 221.55$ K, pressure $P_\infty = 2549.2$ Pa and thermal conductivity $k = 0.0199$ W/m.K. The density is calculated assuming ideal gas and the viscosity is determined using Sutherland's law. The free stream Mach numbers are 6, 8 & 10 corresponding to free stream Reynolds number Re_∞ of 4×10^6 , 5.34×10^6 & 6.67×10^6 , respectively. For wall boundaries, the no-slip condition is imposed and all the walls are isothermal walls with $T_w = 300$ K.

2.4. Flow Solver

The commercial code FLUENT is used to solve the Navier-Stokes equations on the problem domain. The solution is implicit and second order accurate. The flux is calculated using Roe's scheme. Crawford [1] observed that for Reynolds numbers greater than 0.3×10^6 the flow is no longer laminar, hence the Spalart-Allmaras model is employed. The drag coefficient is calculated based on the projected area of the test model, which is a circle with diameter 1 m for all models.

3. Results & Discussion

3.1. Flow field Structure

The underlying concept behind the working of a spike is that it, literally, breaks the strong bow shock, created ahead of a blunt body, to a system of weaker shock waves. As the spike penetrates the flow, ahead of the blunt nose, it causes the flow to separate. This separation is induced by the adverse pressure gradient, created by the blunt nose, which the boundary layer flow can't sustain causing the separation of the shear layer from the surface of the spike. The shear layer, then, reattaches to the blunt body and some of the fluid in it is bled along the way forming a low density (and pressure) vortex structure –called the recirculation zone. Fig. 4 shows the Mach and density contours for a typical spiked hemispherical body equipped with a hemispherical aerodisk.

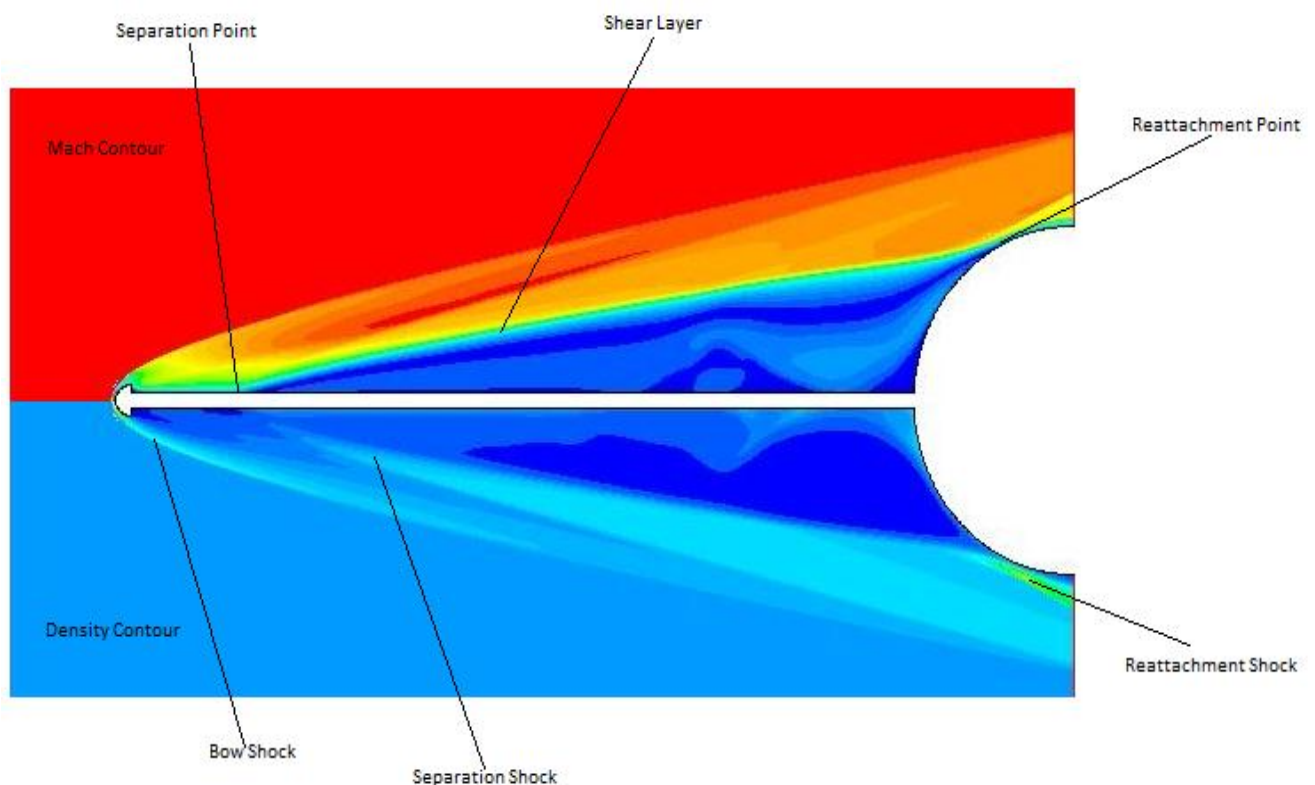


Fig. 4 Flow field around a typical spiked body at Mach 6.

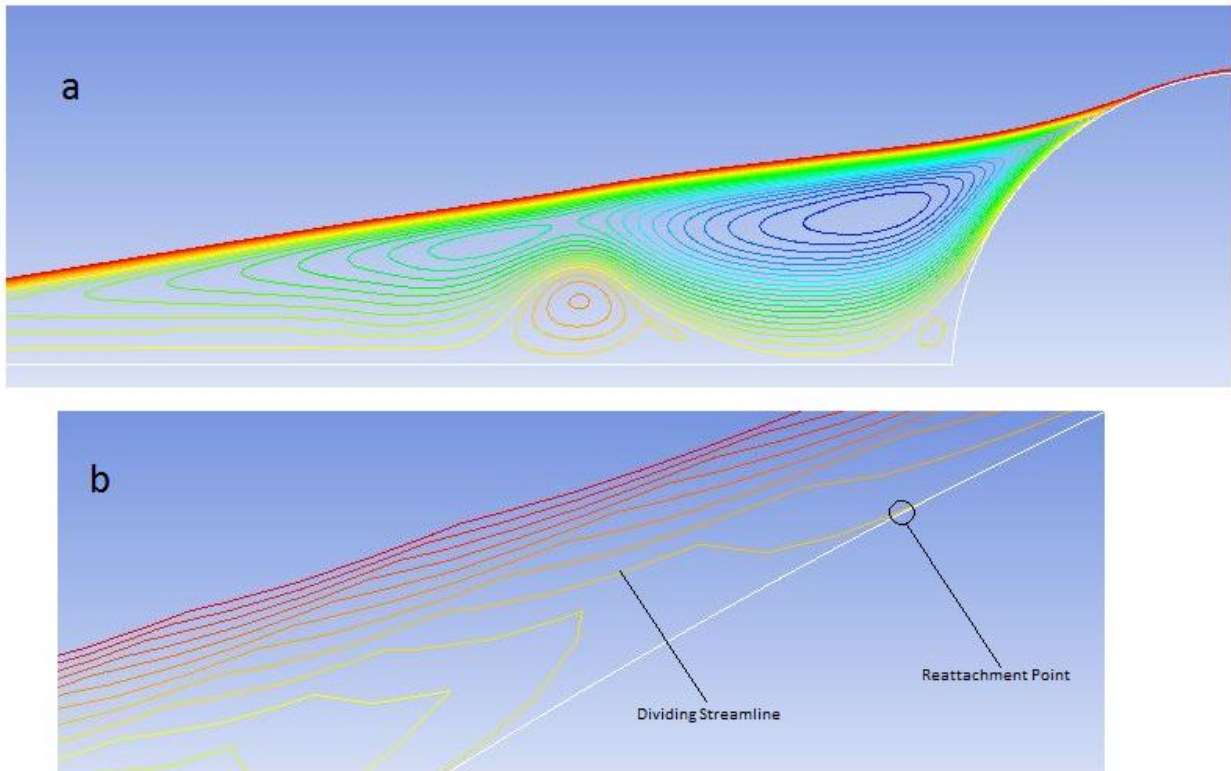


Fig. 5 Recirculation zone ahead of the blunt body: (a) vortex structure; (b) close-up view on the reattachment point.

The shape and size of the recirculation zone determines the amount of drag reduction achieved. MYM Ahmed & N. Qin [6] emphasized the concept of the effective body; that's the effective shape for the whole spiked configuration as seen by the oncoming flow. They found that the effective body is best defined by the dividing streamline (Fig. 5b) which outlines it. In this way, the flow effectively sees the spiked configuration as a more slender close-to-conical body.

The system of shock waves formed by the presence of the spike consists of three shock waves. As the spike penetrates the flow ahead of it, a bow shock wave is formed due to the presence of the spike. The second shock takes place at the separation point, and is called the separation shock, as a result of flow deflection after leaving the surface of the spike. Lastly, the reattachment shock is formed because of flow impingement on the shoulder of the blunt nose. The strength of the latter shock depends on how much the flow is being turned away from the body. Consequently, the farther back the reattachment point becomes, the less drag and heating. The above mentioned system of shocks can be observed by consulting the density contour in Fig. 4.

3.2. Blunt Hemisphere

The blunt hemisphere had $C_D = 0.886, 0.888$ & 0.889 at the three Mach numbers 6, 8 & 10, respectively. The three values differ very slightly. An average value is assumed $C_D = 0.888$ which agrees very well with the value given in [6] of total $C_D = 0.887$. This value ($C_D = 0.888$) represents the reference value with respect to which reductions in drag will be calculated.

3.3. Sharp Spike

The sharp spike investigated herein is tested at Mach 6 corresponding to $Re_\infty = 4 \times 10^6$. This configuration showed very little drag reduction; that's 21.96% ($C_D = 0.692$). It is observed from the Mach contour of this configuration (Fig. 6) that the separation point was retarded because of the high energy that the flow now possesses which kept the flow attached to the spike up to about half of its length. This delay in separation has a shrinking effect on the recirculation zone causing the reduction in the drag to be very little. It's worth stating here that this same configuration has $C_D = 0.21$ at $Re_\infty = 0.13 \times 10^6$ according to the experiment conducted by Crawford [1]. It's also shown in [1] that the amount of drag reduction decreases with increased Reynolds numbers.

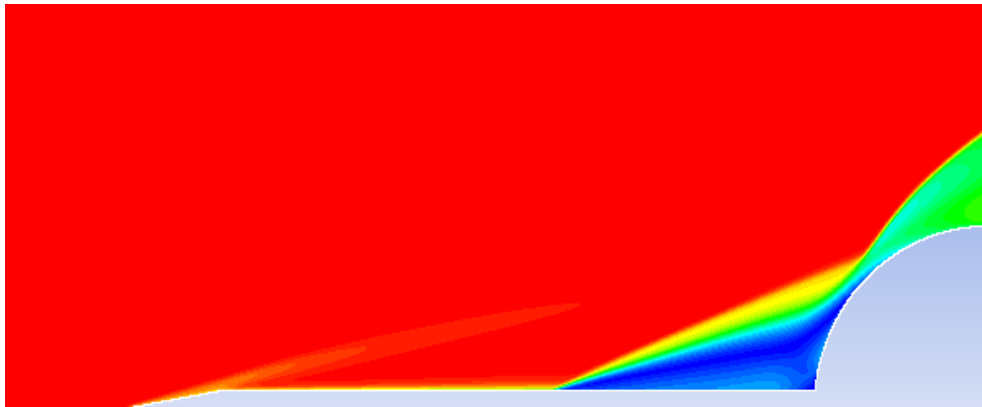


Fig. 6 Mach contour of the sharp spike with $L/D = 2$ at Mach 6.

3.4. Hemispherical Aerodisk

The model tested has $L/D = 2.5$ and $d/D = 0.1$. The same model had been previously tested at $Re_\infty = 3.69 \times 10^4$ and gave total $C_D = 0.118$ [6]. At $Re_\infty = 4 \times 10^6$, however, the effect was much less significant giving $C_D = 0.568$; that's a reduction of 35.89%. Apparently the high Reynolds number along with the more energetic turbulent boundary layer delayed the point of separation, Fig. 7. Thus, less of the body is screened by this low pressure region (recirculation zone) yielding higher drag compared to the value obtained at the lower Reynolds number.

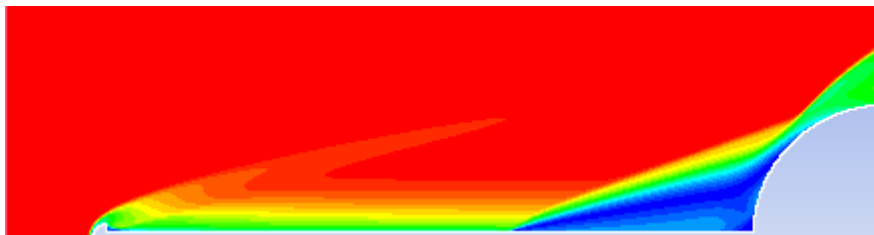


Fig. 7 Mach contour around the hemispherical aerodisk with $L/D = 2.5$, $d/D = 0.1$ at Mach 6.

3.5. Spiked Aerodisk

At Mach 6, this configuration resulted in a drag reduction of 56.28% with $C_D = 0.388$. The resulting flow field is shown in Fig. 9. As the figure reveals, the flow first encounters the smaller spike, and due to the high bluntness of the aerodisk causing high adverse pressure gradient, then it separates and reattaches to the aerodisk. And facing the adverse pressure gradient created by the presence of the hemispherical nose, the flow separates again and reattaches to the shoulder of the hemisphere at an angle of roughly 55° .

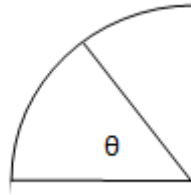


Fig. 8 Angle θ on the fore-body measured from the spike root in a clockwise sense.

This configuration proved to be superior to the sharp spike and the aerodisk-equipped configurations; it succeeded in causing the turbulent boundary layer to separate at the investigated Reynolds numbers. Similar flow fields were obtained at Mach 8 & 10. Table 1 summarizes C_D values as well as their respective reduction percentages and Fig. 10 illustrates the variation of static pressure along the surface of the hemisphere (the angle theta is measured in clockwise direction with zero denoting the spike's root, Fig. 8). The reattachment point takes place at an angle slightly smaller than that where peak pressure occurs; the effect of pressure rise, due to reattachment, lags slightly [6].

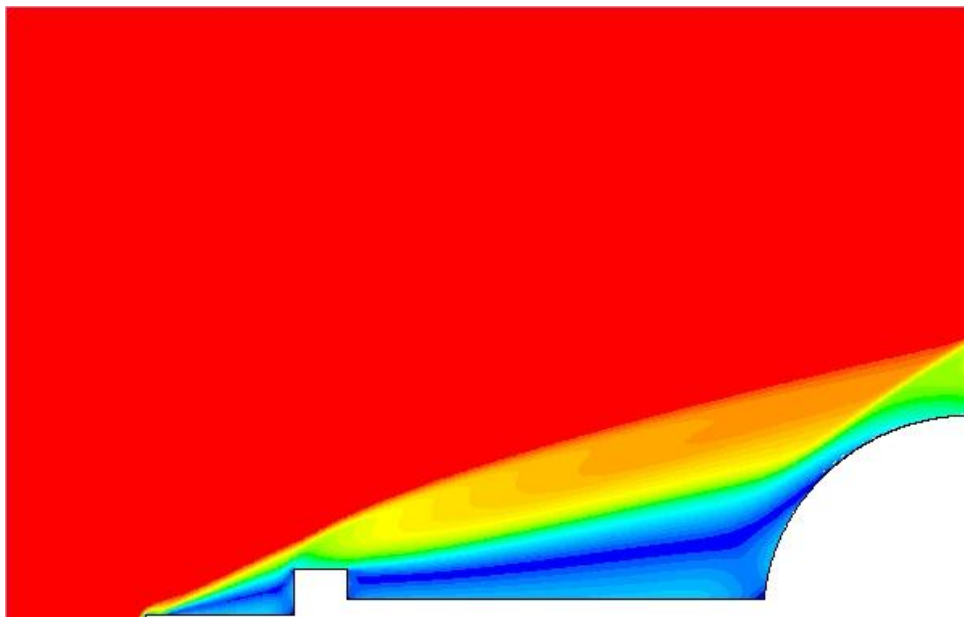


Fig. 9 Mach contour around the spiked aerodisk at Mach 6.

Table 1 Spiked aerodisk C_D values at Mach 6, 8 & 10.

Mach	6	8	10
C_D	0.388	0.397	0.404
Reduction	56.31 %	55.29%	54.5%

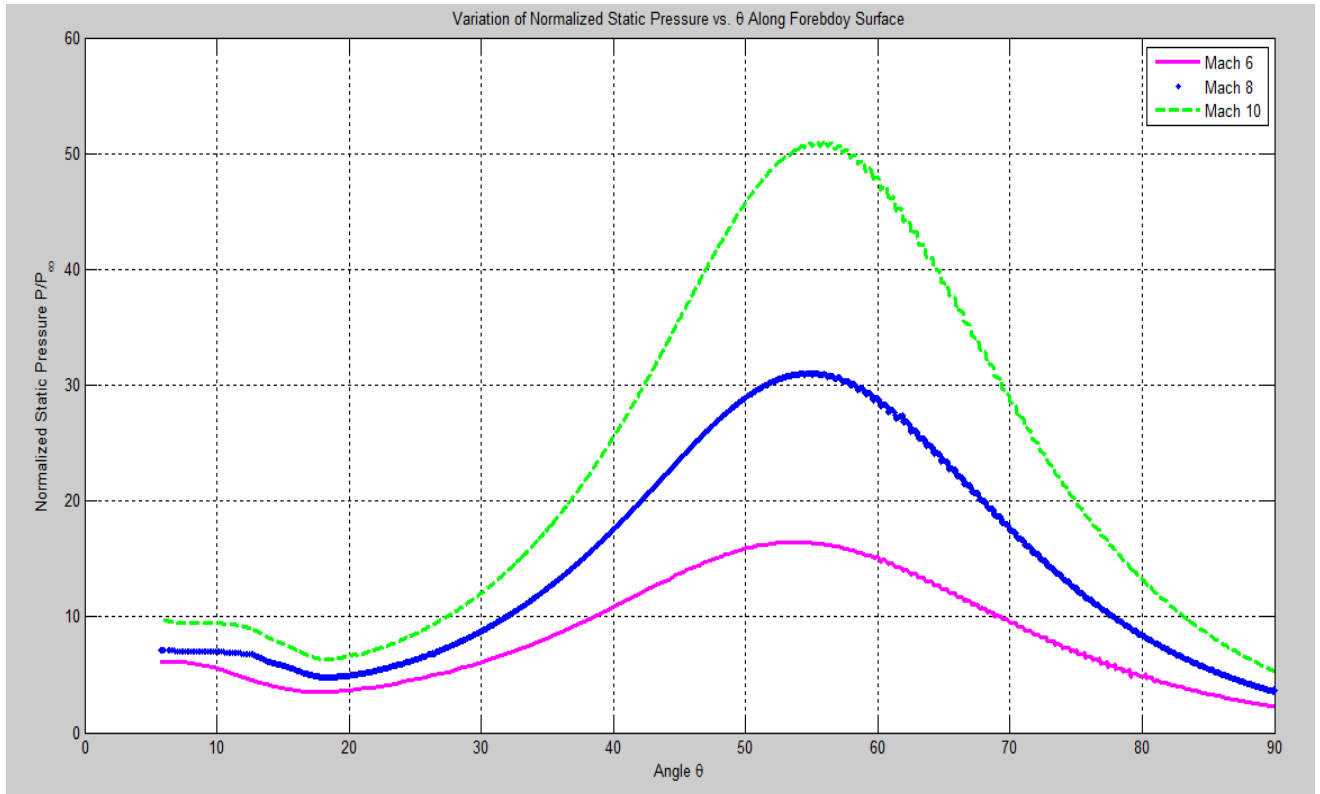


Fig. 10 Variation of static pressure along the surface of the hemisphere at Mach 6, 8 & 10.

The temperature distribution around the spiked aerodisk configuration is shown in Fig. 11. Fig. 12 shows the total heat flux along the fore-body of the same configuration at three Mach numbers. As expected, the heat transfer to the body increases with the increase of Mach number.

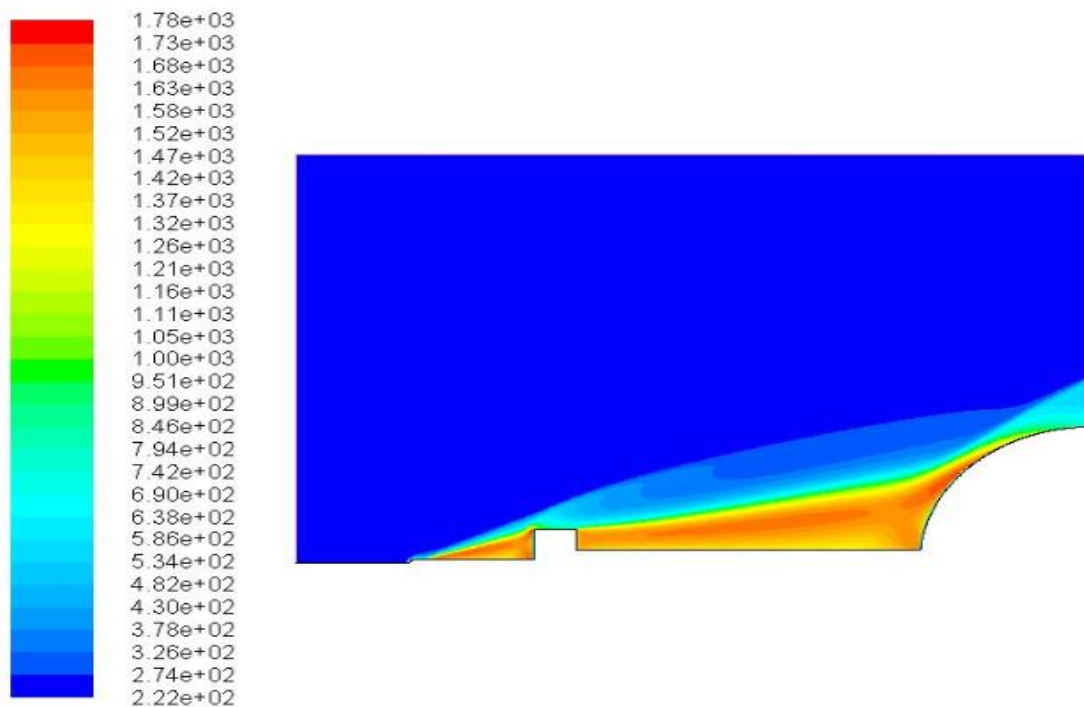


Fig. 11 Temperature contour around the spiked aerodisk configuration at Mach 6 (values given in Kelvins).

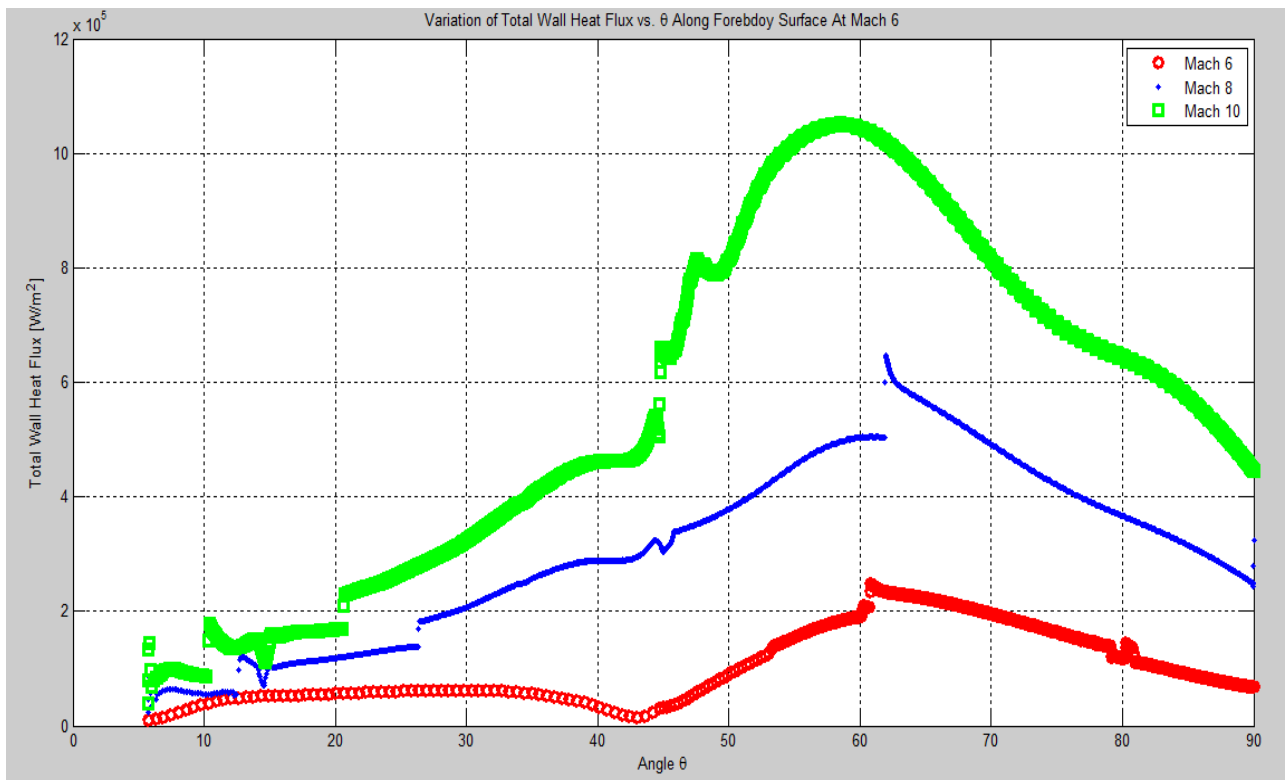


Fig. 12 Total heat flux along the surface of the hemisphere at Mach 6, 8 & 10.

3.6. Reattachment Ring

The ring of height $h = 0.1D$ mounted at the reattachment point (roughly 55°) of the preceding configuration proved its use in alleviating both the static pressure and the heating resulting from the direct impingement of the shear layer upon the shoulder of the nose. Surprisingly, this ring didn't only alleviate the pressure locally, but it also reduced the overall drag by 27.12% of the spiked aerodisk C_D value. Fig. 13 clearly depicts that the recirculation zone is considerably enlarged with the use of the reattachment ring and how it dodges the shock away from the nose.

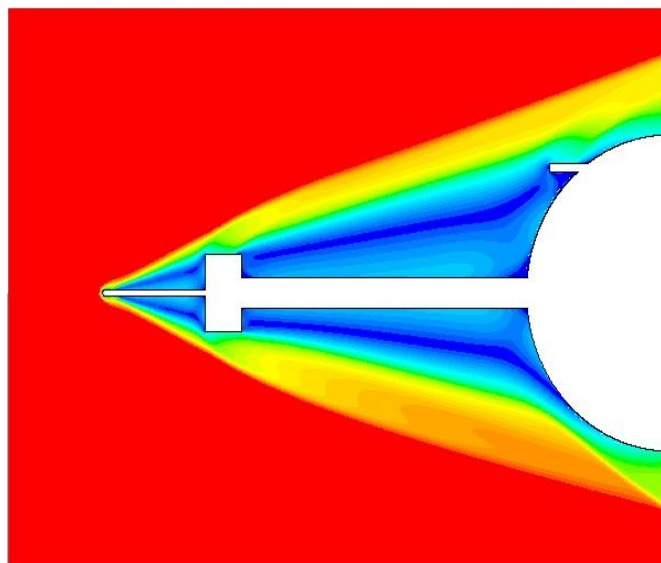


Fig. 13 Mach contour with reattachment ring (upper) and without (lower).

A close-up view (Fig. 14) at the reattachment ring reveals how it works in much the same way as a conventional spike does; it breaks a shock wave to a number of weaker shocks. The temperature contour around this configuration is shown in Fig. 15. Fig. 16 & 17 show how the reattachment ring has superior characteristics in terms of minimizing static pressure and total heat flux on the surface of the hemisphere (the gap in the reattachment ring's plot is attributed to the presence of the ring on the hemisphere; the ring is not included).

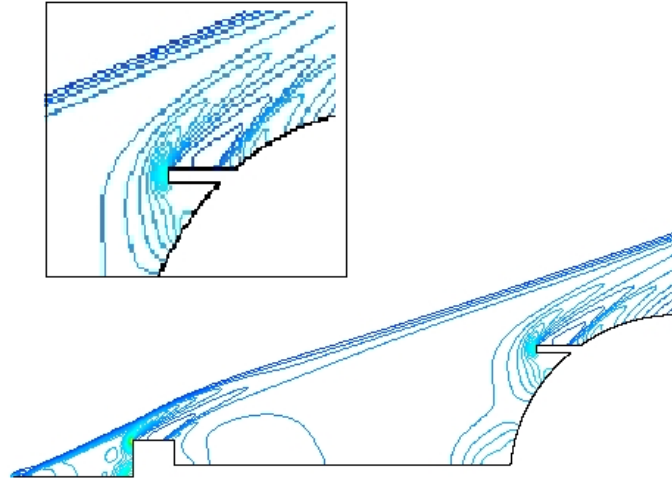


Fig. 14 Pressure contours around the body with a close-up view at the reattachment ring.

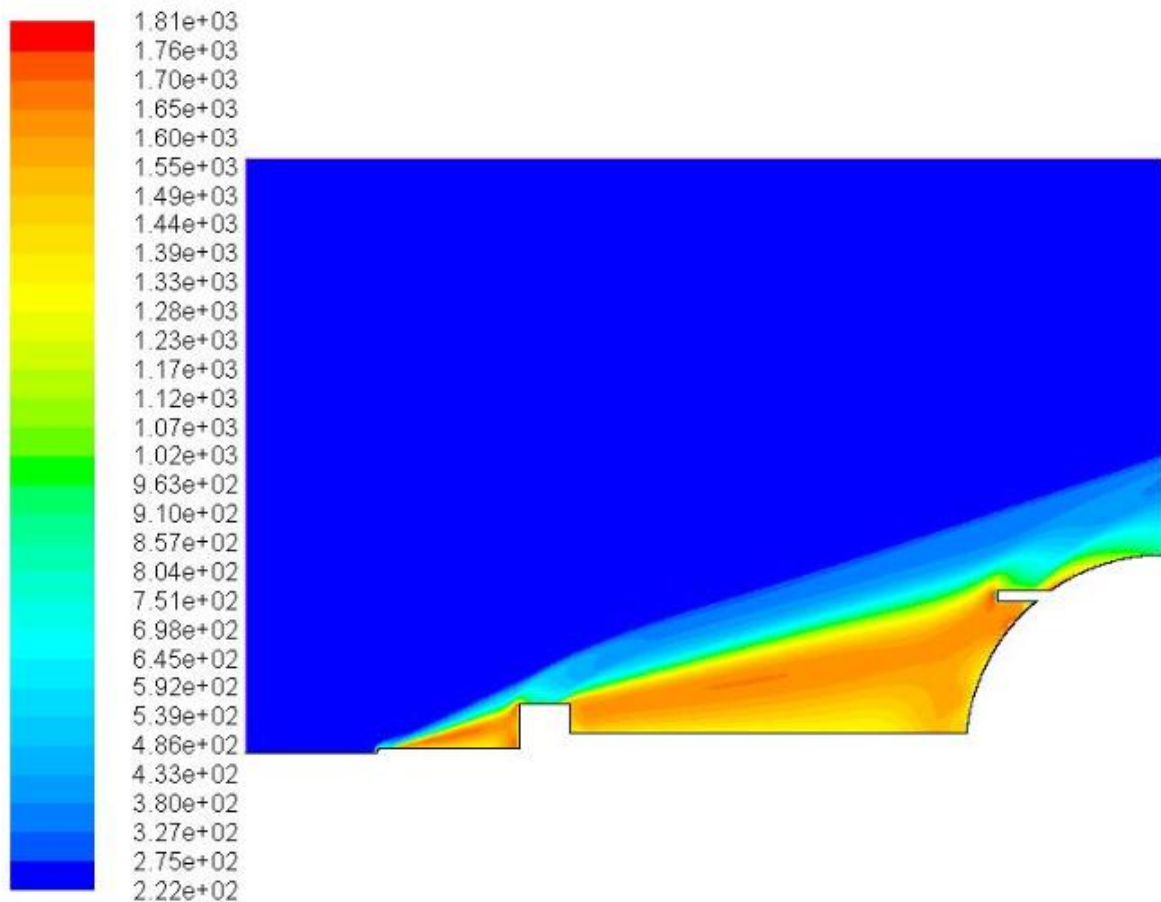


Fig. 15 Temperature contours around ring fitted configuration with $h = 0.1D$ at Mach 6 (values given in Kelvins).

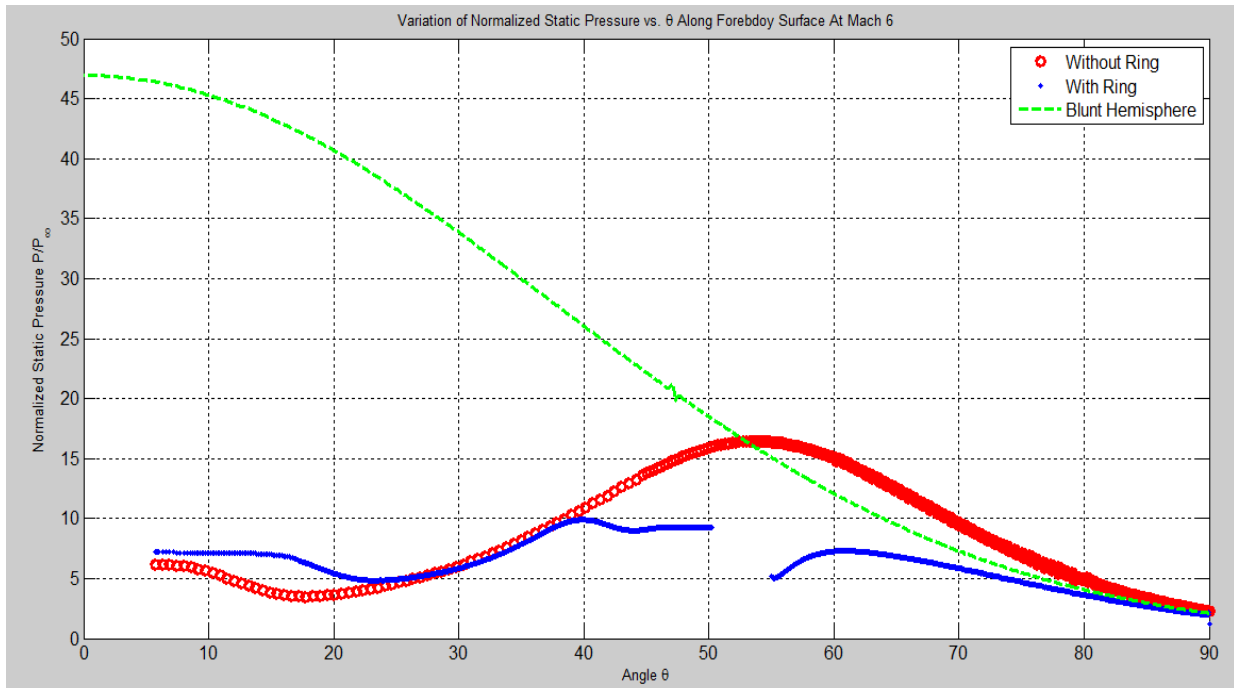


Fig. 16 Static pressure at Mach 6.

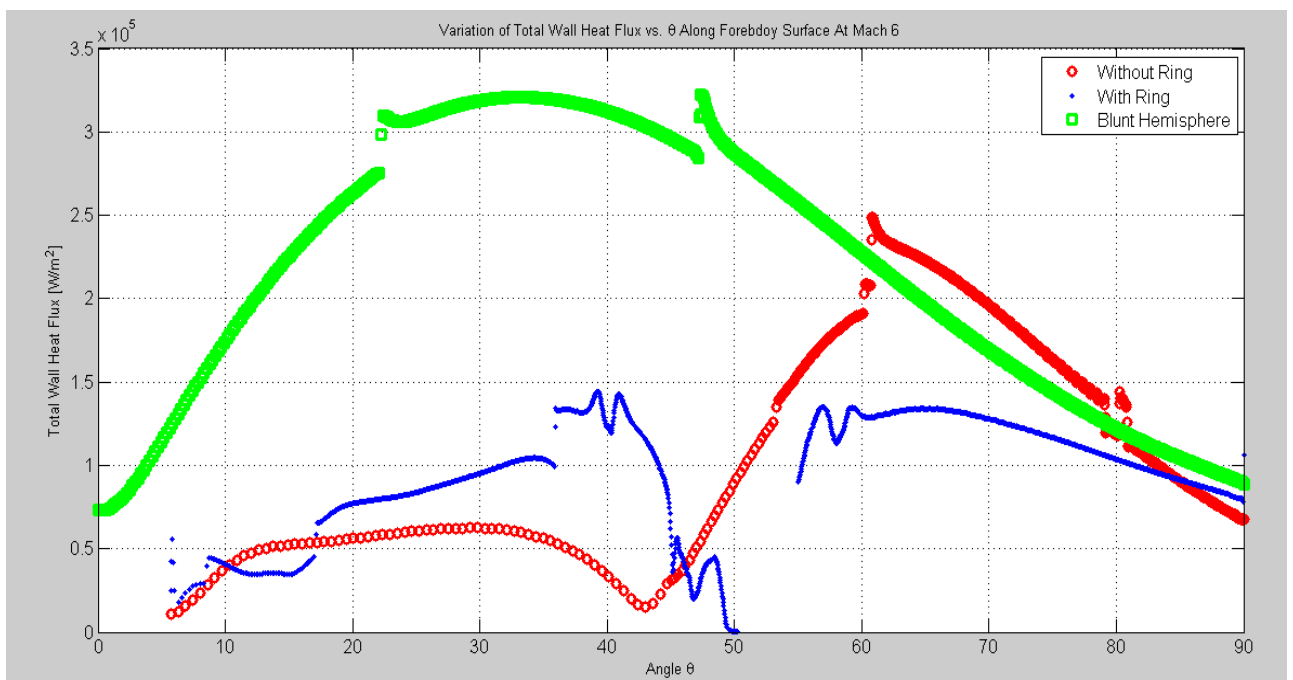


Fig. 17 Total wall heat flux at Mach 6.

The drag varied very slightly at different Mach numbers as shown in Table 2. This result is congruent with the observation made by V. Kulkarni et al. [2]; at hypersonic speeds the percentage of drag reduction is independent of the free stream Mach number and the stagnation enthalpy of the oncoming stream.

Table 2. C_D values for spiked aerodisk, with and without reattachment ring, and overall drag reduction.

Mach	6	8	10
C_D	0.388	0.397	0.404
C_D (with ring)	0.282	0.273	0.268
Overall Reduction	68.24%	69.26%	69.82%

3.6.1. Effect of Ring Height on the Flow field

In order to understand the effect of changing the ring height h on the overall performance of the configuration, two cases were investigated with $h = 0.1D$ & $0.5D$. Fig. 18 shows that the recirculation zone for the case with $h = 0.5D$ is larger than the $h = 0.1D$ case. However this didn't yield lower drag, in fact, this case resulted in higher drag.

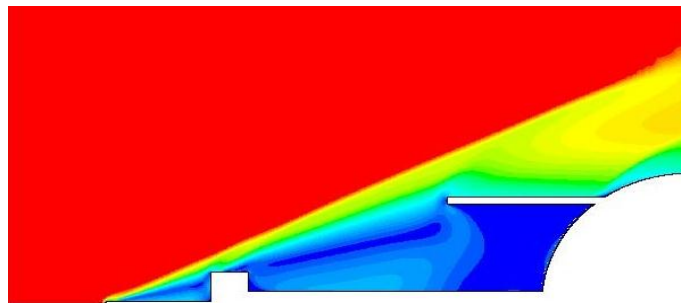


Fig. 18 Mach contour around the ring-fitted assembly with $h = 0.5D$.

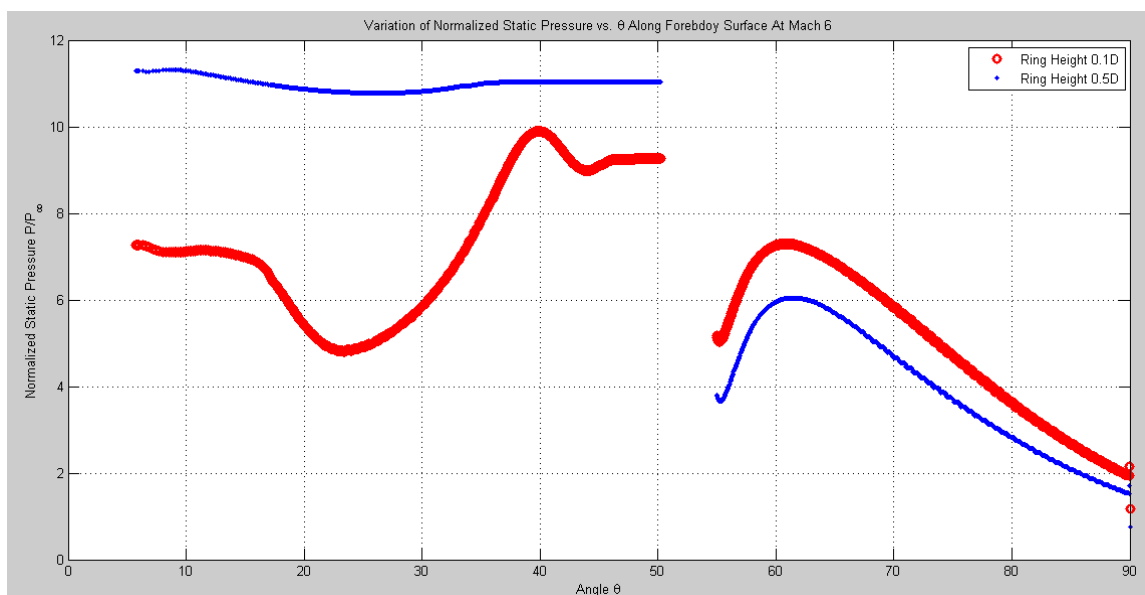


Fig. 19 Static Pressure along the hemisphere surface for $h = 0.1D$ & $h = 0.5D$ at Mach 6.

Figure 19 provides clue of how the drag increased even with the increase of the recirculation area. The static pressure for the case with $h = 0.5D$ is higher than that for $h = 0.1D$ up to an angle of about 50° . This high pressure region is the result of the ramming effect exerted by the flow upstream on the fluid in the recirculation zone (which is now trapped in the cavity formed by the presence of the ring). The force, resulting from the presence of high pressure fluid in this area, when resolved to its components the axial component dominates. On the other hand, looking at the area from $\theta = 55^\circ$ to $\theta = 90^\circ$ we observe that the ring with $h = 0.1D$ has higher static pressure on the nose. And because at such angles the dominant component is the radial one, the drag value is not so much affected.

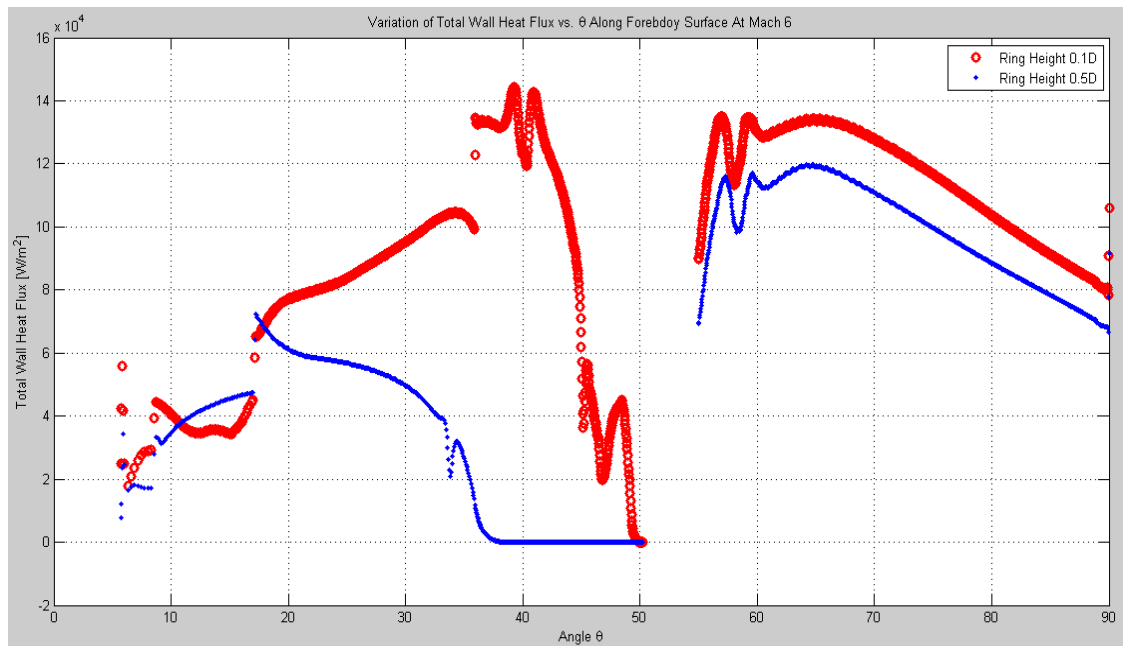


Fig. 20 Total heat flux along the hemisphere surface for $h = 0.1D$ & $h = 0.5D$ at Mach 6.

From a heat reduction view point, the two heights also gave different effects. Consulting Fig. 20, it's evident that the case for $h = 0.5D$ yielded lower heat flux to the fore-body for almost the whole surface. The heat flux for this configuration exhibits a very interesting behavior; it flattens out at a near zero value for the angles from about 38° up to 50° . Fig. 21 provides an answer for why this is. As shown, the temperature distribution at the surface of the hemisphere at this angle range takes on a value very close to that of the wall, hence very little (close to zero) heat transfer takes place at this area. In fact, heat transfer in this area is from the body, which has higher temperature, to the fluid. The maximum value for the total heat flux at this area is 0.465 W/m^2 .

The above discussion shows that in determining the optimal height of the reattachment ring there must be a trade-off between attaining maximum drag and heat reduction. By understanding the effect of the ring's height on the flow field, tailored configurations can be sought in order to meet the preset requirements of specific hypersonic flights.

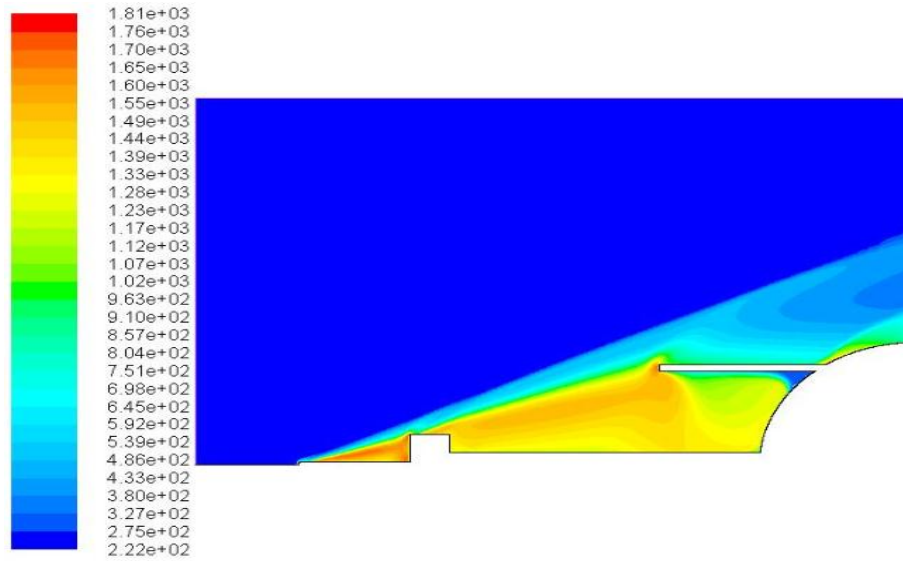


Fig. 21 Temperature contour around the ring fitted configuration for $h = 0.5D$ at Mach 6 (values given in Kelvins).

4. Comparison with Previous Investigations

The results obtained in this study are now compared with other findings in the literature at different Reynolds numbers. Table 3 shows the maximum percentages of drag reduction achieved in [6,8,5] along with the two maximum reduction percentages obtained in this work for the spiked aerodisk and the ring-fitted configurations. As shown, the percentage drag reduction deteriorates with increased Reynolds number. The ring-fitted configuration, however, shows an exceptional performance; it attained a drag reduction equivalent to that attained at $Re_\infty = 1.5 \times 10^6$.

Table 3. Maximum drag reduction percentages compared with previous investigations.

Re_∞	3.69×10^4	1.5×10^6	2.26×10^6	4×10^6	6.67×10^6
C_D Reduction	86.7%	70%	62.73%	56.3%	69.82%
Source	[6]	[5]	[8]	Spiked Aerodisk	Ring-Fitted Assembly

5. Conclusions

Two novel concepts for drag and aerodynamic heating reduction were presented in this work: the spiked aerodisk assembly and the reattachment ring. The two configurations were tested at free stream Mach numbers 6, 8 & 10. The spiked aerodisk configuration showed superiority over the two conventional configurations tested with maximum drag reduction of 56.31%. The flow field around this configuration showed it could cause the oncoming flow to separate more effectively than the normal hemispherical aerodisk and the sharp spike. The flow at such high Reynolds number is turbulent; separation is harder.

The reattachment ring proved to be very beneficial in terms of heat and drag mitigation. Maximum drag reduction of 69.82% was achieved with this configuration at Mach 10. This concept reduced the static pressure on the surface of the blunt hemisphere accompanied by a significant decrease in the peak heating value. It was observed that by altering the height of the reattachment ring, tailored mission-specific configurations can be produced to meet preset drag and heating objectives.

6. Recommendations

The authors recommend an optimization study on the spiked aerodisk to come up with the optimal dimensions for maximum drag reduction. The reattachment ring concept needs further research to optimize its performance, and in particular, its performance at non-zero angles of attack. Control and stability concerns need to be addressed to determine the feasibility of both concepts in real flights.

7. References

- [1] Crawford, D.H., "Investigation of the Flow over a Spiked-Nose Hemisphere-Cylinder at a Mach Number of 6.8," NASA-TN-D-118, Dec. 1959.
- [2] Kulkarni, V., Menezes, V., Reddy, K.P.J., "Effectiveness of Aerospikes for Drag Reduction on a Blunt Cone in Hypersonic Flow," *Journal of Spacecraft and Rockets*, Vol. 47, No. 3, May-June 2010.
- [3] Khlebnikov, V. S., "Effect of Periodic Disturbances on the Flow in a Nonsymmetric Separation Zone ahead of a Blunt Body," *Fluid Dynamics*, Vol. 31, No. 5, 1996, pp. 731-738.
- [4] Kobayash, H., Maru, Y., Hongoh, M., Takeuchi, S., Okai, K., Kojima, T., "Study on Variable-Shape Supersonic Inlets and Missiles with MRD Device," *Acta Astronautica* 61 (2007), pp. 978-988.
- [5] Schülein, E., "Wave Drag Reduction Concept for Blunt Bodies at High Angles of Attack," *Berlin Heidelberg: Springer*, 2009, pp. 1315-1320.
- [6] Ahmed, M.Y.M., Qin, N., "Drag Reduction Using Aerodisks for Hypersonic Hemispherical Bodies," *Journal of Spacecraft and Rockets*, Vol. 47, No. 1, 2010, pp. 62-80.
- [7] Ahmed, M.Y.M., Qin, N., "Recent Advances in the Aerothermodynamics of Spiked Hypersonic Vehicles," *Progress in Aerospace Sciences* 47, 2011, pp. 425-449.
- [8] Gauer, M., Paull, A., "Numerical Investigation of a Spiked Blunt Nose Cone at Hypersonic Speeds," *Journal of Spacecraft and Rockets*, Vol. 45, No. 3, 2008, pp. 459-471.
- [9] Salim, S.M., Cheah, S.C., "Wall y^+ Strategy for Dealing with Wall-bounded Turbulent Flows," *Proceedings of the International MultiConference of Engineers and Computer Scientists*, IMECS 2009, Vol. II, 2009.
- [10] Versteeg, H.K., *An Introduction to Computational Fluid Dynamics – The Finite Volume Method*. 2nd edition, Pearson Education Limited, 2007, pp. 275.
- [11] "U. S. Standard Atmosphere, 1976" NASA TM-X-74335, 1976.